THIRTEENTH EUROPEAN ROTORCRAFT FORUM

Paper No. 65 2.17

MODEL ROTOR WAKE MEASUREMENTS IN A WIND TUNNEL

B. Junker

Deutsche Forschungs- und Versuchsanstalt
für Luft- und Raumfahrt e. V.,
Institut für Flugmechanik
Braunschweig, Germany

W. Gradl, V. Mikulla
Messerschmitt-Bölkow-Blohm GmbH
Munich, Germany

September 8-11, 1987
Arles, France

ASSOCIATION AERONAUTIQUE ET ASTRONAUTIQUE DE FRANCE

MODEL ROTOR WAKE MEASUREMENTS IN A WIND TUNNEL

B. Junker

Deutsche Forschungs- und Versuchsanstalt
für Luft- und Raumfahrt e. V.,
Institut für Flugmechanik
Braunschweig, Germany

W. Gradl, V. Mikulla
Messerschmitt-Bölkow-Blohm GmbH
Munich, Germany

Abstract

The present paper reports the results of detailed measurements of the induced velocity field in the rotor wake of a 4 m diameter model rotor mounted in the DNW - wind tunnel. Advance ratios ranged from Hover to $\mu = 0.25$ and included simulated ascent and descent flight cases. The measurements consisted of triple hot wire sensor data of the steady and unsteady components of the induced velocity in five different parallel planes below the rotor disc.

A direct comparison between the measured induced velocities and calculated induced velocities with a prescribed vortex model program in the rotor disc plane was difficult and uncertain firstly because of a necessary extrapolation of the measurements from planes underneath the rotor into the rotor plane and secondly because of experimental uncertainties due to unknown interference effects between the rotor inflow and the surrounding wall boundaries.

While the extrapolation of the hot wire measurements into the rotor plane gave reasonable agreement with the calculation of the instantaneous induced velocities for some flight cases and specific azimuthal positions there was in general better agreement between calculation and direct measurements in a plane 10 cm below the rotor and here in particular for the transition flight case.

Notation

c_a	profile lift coefficient
c_T	thrust coefficient
F	force acting on rotor hub
G	weight
M	moment acting on rotor hub
n	number of blades
N	rotor power
p	pressure
r	radial coordinate
R	radius of rotor
S	rotor thrust

t	temperature
t	blade chord
t	time
V	velocity
w	induced velocity
X, x	cartesian coordinates
Y, y	
Z, z	
α_{eff}	effective angle of attack
α_{Ro}, θ_L	rotor disc angles of incidence
φ	yaw angle
Γ	circulation
θ_0	collective pitch angle
θ_c, θ_s	cyclic control angles
μ	advance ratio
ρ	density
ψ	azimuth angle

Indices

i	induced
M	model
max	maximum
RES	resultant
x, y, z	cartesian coordinates

1. Introduction

Because of its fundamental importance to predict rotor performance, structural limitations, vibrations, stability and acoustic characteristics there have been quite a few experimental and even more theoretical investigations of rotor induced velocity fields and rotor wake flow phenomena in the past.

Nevertheless there is still a need for more accurate and complete measurements of rotor induced velocities firstly because the overwhelming amount of data has been limited to the Hovering rotor and secondly because a more complete set of data could guide the empirical input thereby enhancing the accuracy of relative simple but fast prescribed wake models and associated computer codes.

Despite the fact that detailed kinematic and free wake models have been developed in recent years and that the availability of super computers has reduced the calculation time of programs based on these models to acceptable orders of magnitude, industry would still benefit from simple but fast and accurate prescribed wake models for routine rotor calculation and preliminary rotor lay out work. A practical method to improve the accuracy of semi-empirical downwash methods is the accurate experimental determination of the induced velocity field at the rotor blades. While laser doppler anemometry has made it possible to measure instantaneous velocities non-intrusively, it is not a cheap measurement technique and far from a routine measurement in large wind tunnels. In the present program it was therefore attempted to obtain detailed measurements of the induced velocity field below a model rotor

with hot wire probes by making use of their direction sensitivity.

2. Experimental arrangement

2.1 Model

The model rotor with the exception of a new profile design and shape is basically a 40 % scaled down model of a four-bladed, hingeless BO-105 rotor. The model rotor has a diameter of 4000 mm. The new shape of this blade is a rectangular trapezoidal wing (Fig. 1) with two newly designed profiles [1].

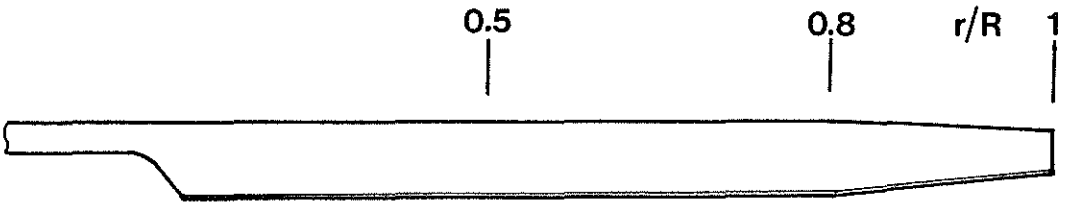

Fig. 1: Rotor Blade

The basic geometric rotor blade parameters are as follows:

rotor diameter [m]		**4**
blade chord [m]	$\frac{r}{R} \leq 0.8$	**0.135**
	$\frac{r}{R} = 1.0$	**0.081**
twist, linear [°/m]		**-5**
blade profile	$\frac{r}{R} \leq 0.8$	**DM-H4**
	$\frac{r}{R} = 1.0$	**DM-H3**
profile beginning from shaft axis [m]		**0.44**
preconing [°]		**0.0**
solidity		**0.077**

Table 1

In contrast to the rectangular blades of the BO-105 model rotor, this rotor will cause weaker tip vortices.

2.2 Wind Tunnel

The tests were conducted in the DNW-wind tunnel. The DNW is a subsonic, atmospheric wind tunnel of the closed return type. It has three interchangeable, closed test section configurations (6 x 6 qm, 8 x 6 qm, 9,5 x 9.5 qm) and one open jet configuration (8 x 6 qm). After erecting and checking the support some hover tests were conducted in the experimental hall with the rotor and measurement support mounted on the wind tunnel section ground floor. The tests with advance ratios greater than zero were carried out in the closed 8 x 6 qm test section of the wind tunnel.

2.3 Measuring Equipment

The rotor rig is a support fixed to the ground floor. Variation of the rotor disc angle of incidence is made possible by a bearing in this support. The rotor is driven by a 100 kW hydraulic motor. The forces and the moments are measured with a six component balance which contains separate measuring elements for stationary and unstationary load components. For the measurement of the rotor torque a separate torque measuring shaft is incorporated in the drive shaft. The actual value of the rotor angle of rotation is given by an azimuth indicator. The rotor blades are equipped with strain gauges for measuring the flapping, lagging and torsional moments. The rotating measuring system on the rotor head acquire the signals of the strain gauges on the blades, on the control rods, on the rotor shaft (bending moment), and of the blade root potentiometer (blade pitch angle). The signals are transmitted to a PCM-facility mounted on the rotating rotor head. After multiplexing, sampling and A/D conversion the data are formatted into a serial data stream for transmission to the ground data acquisition system via a slip-ring set.

The facility to measure the downwash is installed on both sides of the test stand. The probes move over a sliding carriage system in the x- and y-direction. A telescopic mast provides the movement in the z-direction. The measuring equipment is presented in Fig. 2 and 3.

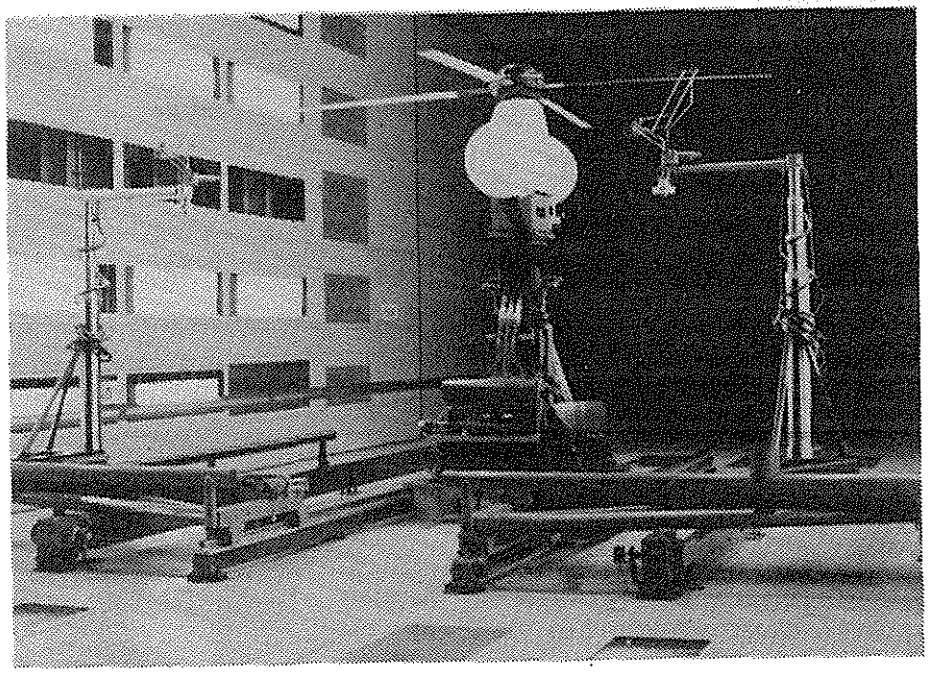

Fig.2: Rotor Test Stand in 6 x 8 m Test Section of DNW-tunnel

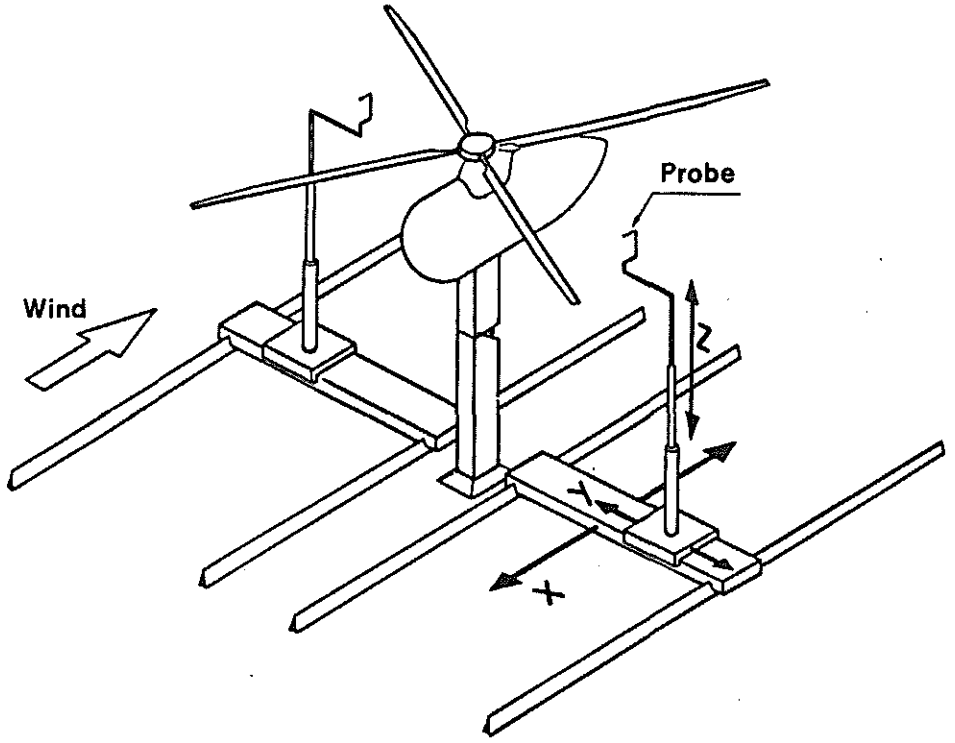

Fig. 3: DFVLR Rotor Test Stand with the Downwash Measuring Equipment

The driving range of the probe includes the rotor disc area with additional movement range in the rear zone (Fig. 4).

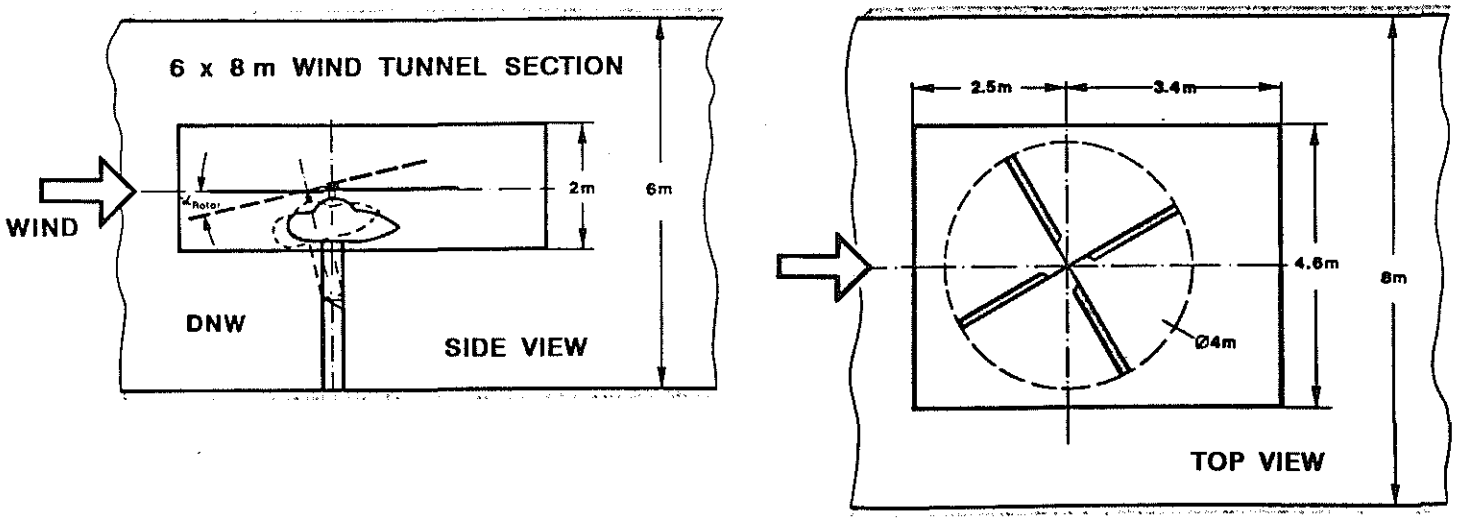

Fig. 4: Measurement Range of the Probes

The measurement region in the z-direction changes with the adjustment of the angle of the rotor-disc. The sliding carriages for the x- and y-movements are driven with chains by regular alternating-current motors with brakes. The z-drives are spindel mechanisms with the same type of motor. The positions of the support and therefore the positions of the probes are measured by potentiometers. The supports are controlled in all directions with a maximum position error of ± 5 mm. This inaccuracy is determined by the type of motor. The error in the measurement position of the potentiometer is in the range of 1 mm. This control error can be ignored with respect to the size of the rotor.

For controlling the support an LS1 11-36 computer was used and special software was developed. The two sensors on the right and on the left were controlled and moved simultaneously. Different control programs were in use. For the experiments with advance ratios greater than zero a program for movement control was available in cartesian coordinates whereas for the hover tests a control for movement in the polar system was used. The centre of the coordinate systems was the rotor centre (Fig. 5).

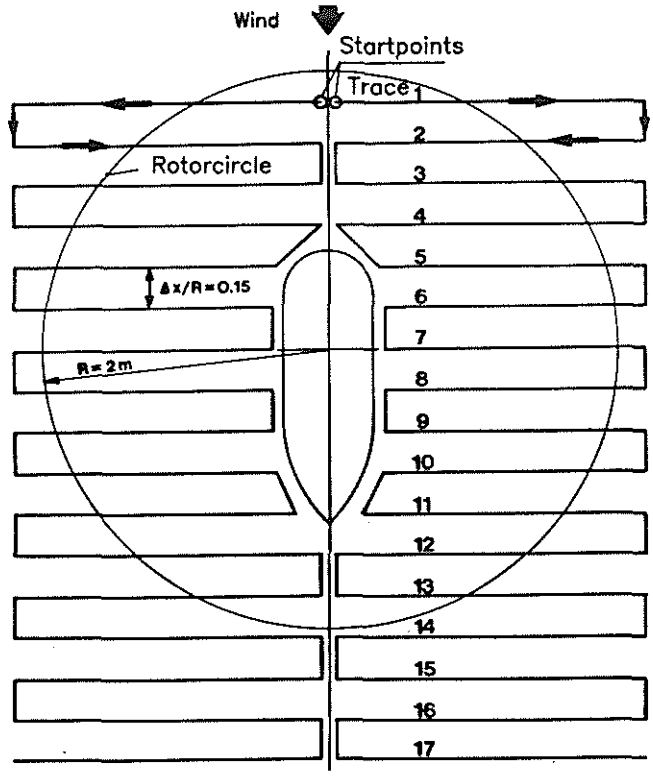

Fig. 5: Traces of the Probes below the Rotor

2.4 The Probe System and the Measuring Principle

The dynamic downwash components beneath the rotor were measured with hot wire probes. Because the probes measure only at defined points, it was necessary to use another method to locate the tip vortices. This was done by dynamic pressure probes. The pressure results were useful for a better understanding of the rotor downwash structure and of the plotted quick look values of the measured flowfield obtained by the hot wire probes. In [2] and [3] the method and the results are presented.

The hot wire sensors consisted of 3 single wires (Fig. 6). Each wire had a vertical position with respect to the plane formed by the other two. The axis of symmetry in this system was the major axis of the probe. Reliable measurements were only possible in a cone section of 70 degrees aperture angle, that means at a yaw angle of 35 degrees with respect to the major axis of the probe. To investigate the whole flowfield beneath the rotor it was necessary to turn the probe such that its major axis was aligned in the direction of mean velocity.

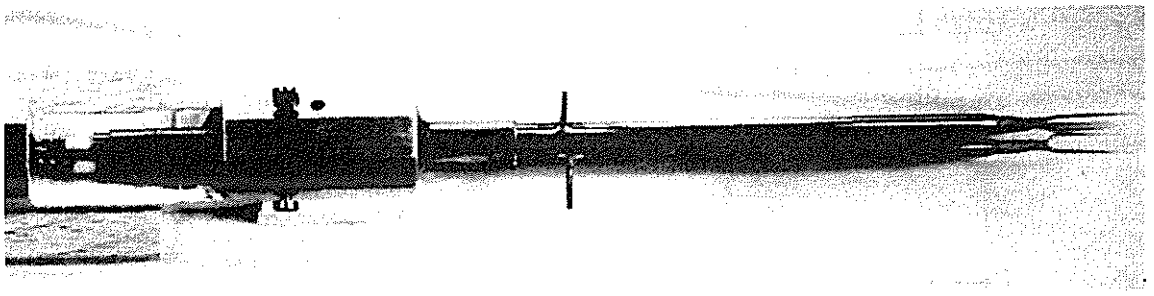

Fig. 6: Triple Hot Wire Sensor

Special probe supports were developed (Fig. 7).The hot wire probes were adjustable in nearly all directions without a change of the position of the sensor top. The information about the sight angle of the probe was given by potentiometers.

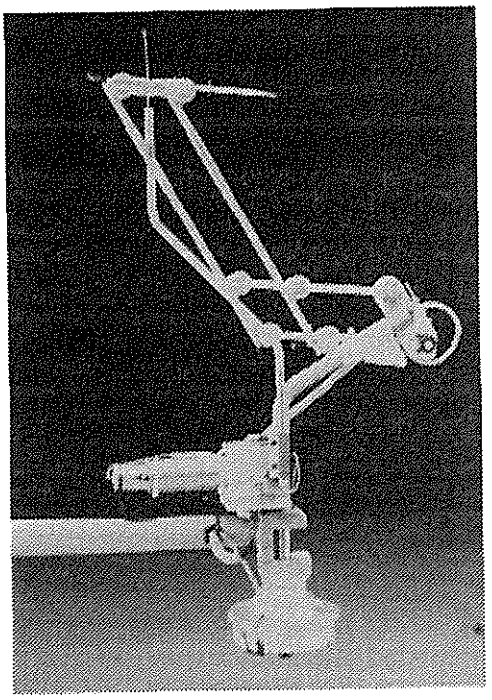

Fig. 7: Hot Wire Sensor Equipment

The LSI 11-36 computer controlled the probe orientation with the help of a specially developed control interface. The purpose of the control circuit (Fig. 8) was to achieve a balance in the signals of two wires (wire 1 and 3) by turning around the z-axis. After this a balance in the voltage level with the last wire could be accomplished by turning around the z-axis.

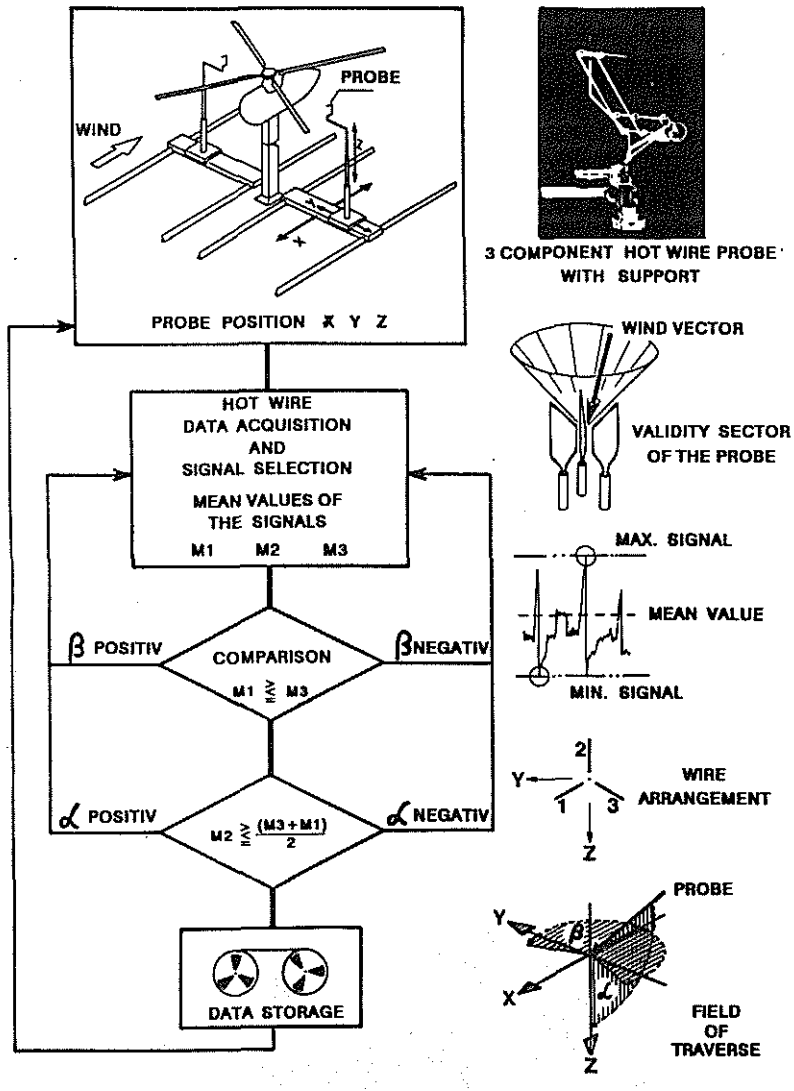

Fig. 8: Principle of the Control Logic for the Probe Orientation

The hot wire anemometers used were developed by the DFVLR and industrially manufactured. These anemometers had a large dynamic measuring range of more than 50 kHz, a linear output and they were controllable by computer.

2.5 Data Acquisition

Parallel to the signals of the anemometers, the position and the sight angles of the probe as well as the azimuth signal of the rotor were recorded on two analog tape recorders over a time period of 10 sec. for one test point. During this recording time the data acquisition path of the rotor test stand recorded all the other signals from the rotating and fixed rotor system including the anemometer and probe support signals.

The signal resolution of the data acquisition system for the rotor test stand was limited by the scanning rate of the PCM-System. The signal limit was 140 Hz which corresponds to the 8. harmonic of the rotor. This was not high enough for a dynamic investigation but satisfactory for quick look data. For further data interpretation the analog signals were digitized with a resolution of 2 kHz. A higher resolution was not efficient.

Fig. 9 gives an overview of the downwash data acquisition.

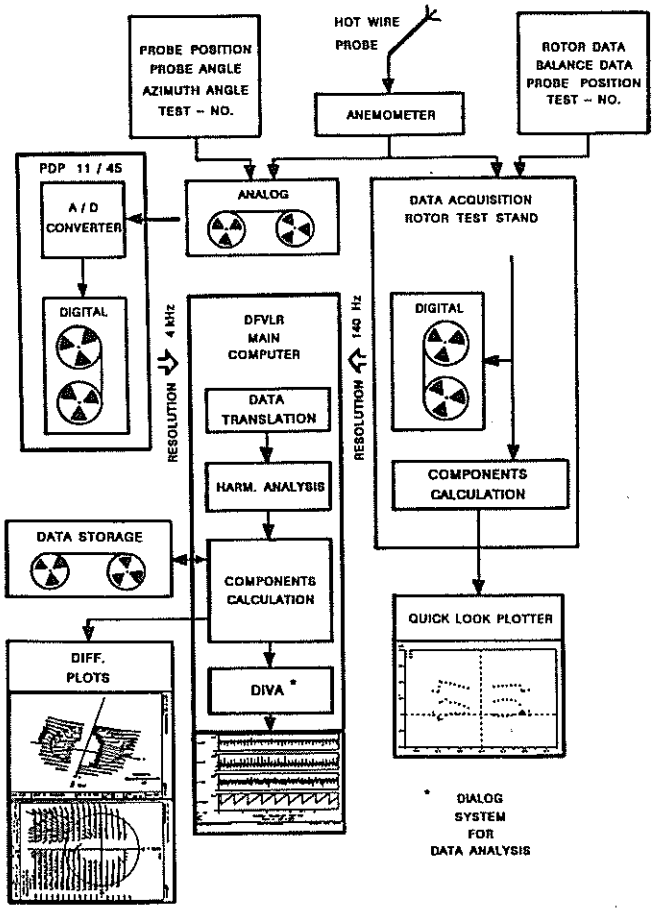

Fig. 9: Data Stream of Hot Wire Measurement

Fig. 10 gives an example of the time history of the three induced velocity components. The orientation of the axes corresponds to the rotor plane axis system.

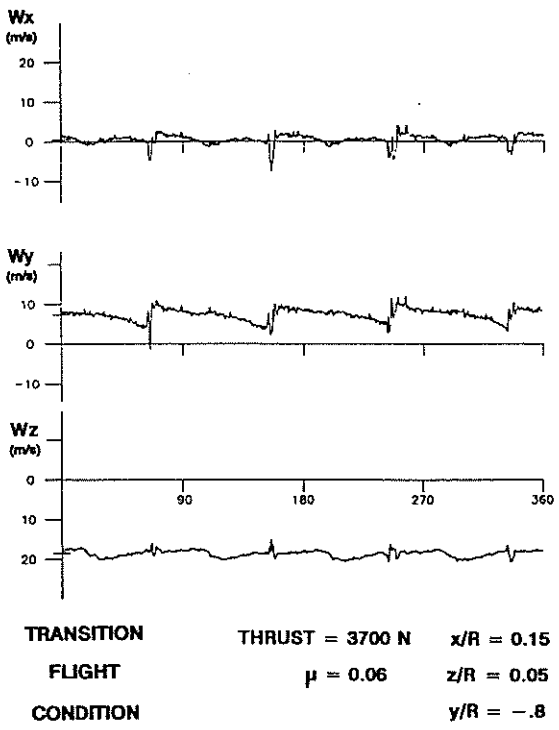

Fig. 10: Induced Dynamic Downwash Components

The results shown in the quick look and in the further data interpretation were calculated from the three hot wire signals.

Many different graphical representations are possible with the great amount of data. Some of them are shown in the following figures. Fig. 11 presents the induced downwash components with their mean value and their dynamic range. The test case was a transition simulation. On top of the figure the signals of the pressure probes are shown.

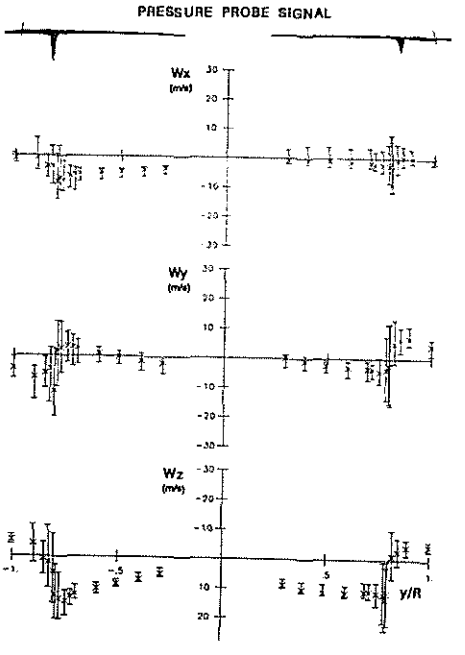

Fig. 11: Induced Mean Downwash Components with Dynamic Range

Another representation is given in Fig. 12. The xy-vector is drawn in the z/R = 0.1 plane.

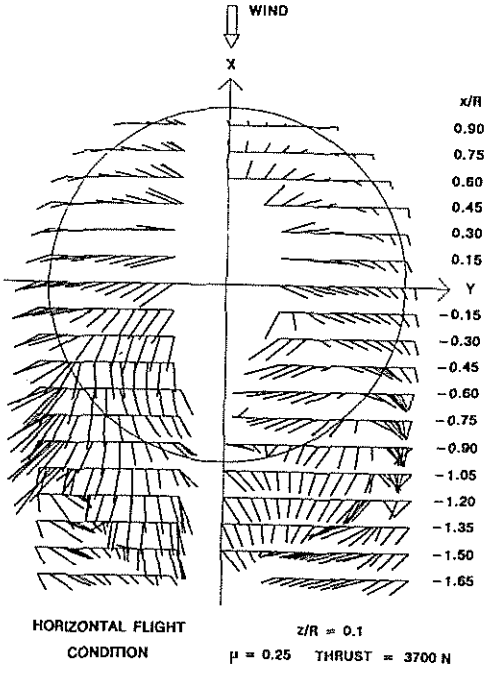

Fig. 12: Induced xy-Downwash Components

Figures 13, 14 and 15 present the induced downwash zy-vector in different x/R sectional drawings. The figures give excellent information about the downwash contraction and the vortex region.

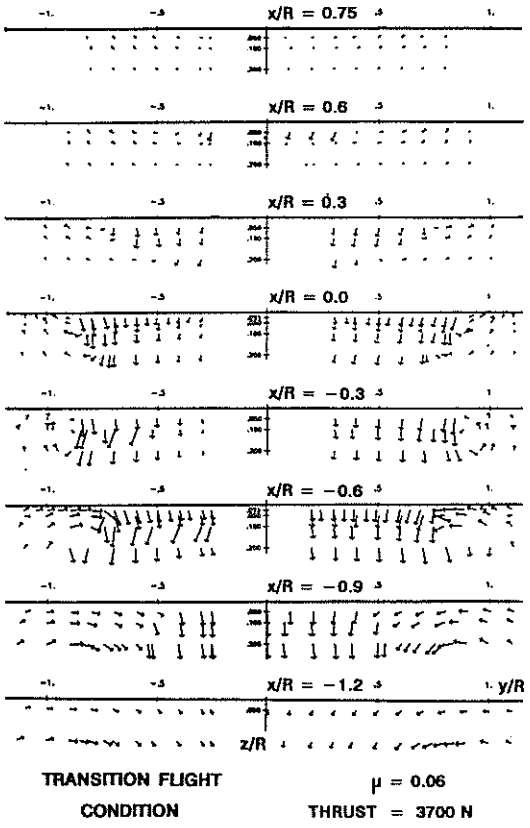

Fig. 13: Induced Downwash Components (Transition flight)

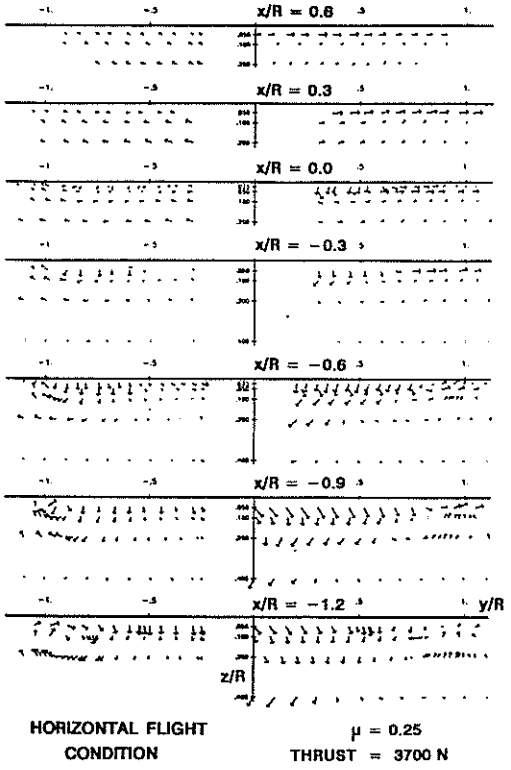

Fig. 14: Induced Downwash Components (Horizontal flight)

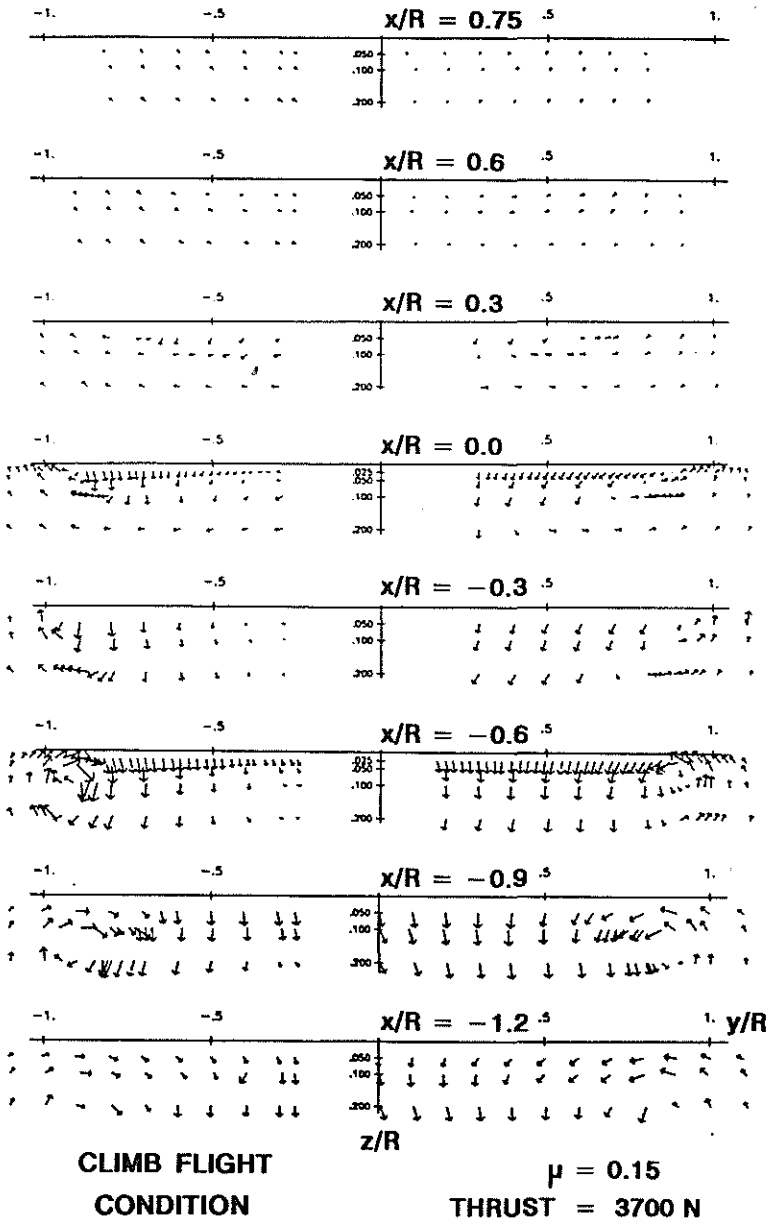

Fig. 15: Induced Downwash Components (Climb)

3. Vortex Model with Prescribed wake geometry

While 'free wake models' as described in [4] and [5] probably lead to the most accurate prediction of rotor induced velocities the 'prescribed wake' models have the important advantage of low computing time and are therefore particularly suited for parametric rotor studies. Their semi-empirical character offers the possibility to increase the accuracy with the help of accurate measurements of the rotor induced velocity field.

The present model is an extension of the numerical procedure described in [6] and [7]. After adjusting some of the program parameters according to the existing measurements the vortex model was modified to include calculation below the rotor disc plane.

In the prescribed vortex model the rotor blades are considered as lifting lines whose bound vortex is divided radially into a finite number of bound vortex segments of different circulation strengths. The difference in circulation strength of neighbouring bound vortex segments

on the blade determines the circulation strength of each discrete shed and trailed vortex filament in the near wake. Shed vortices parallel to the blade radius created as a result of circulation changes with azimuth angle are hereby neglected. The condition of tangential flow off the blade is fulfilled on the lifting line in the centre of each bound vortex segment (Figure 16).

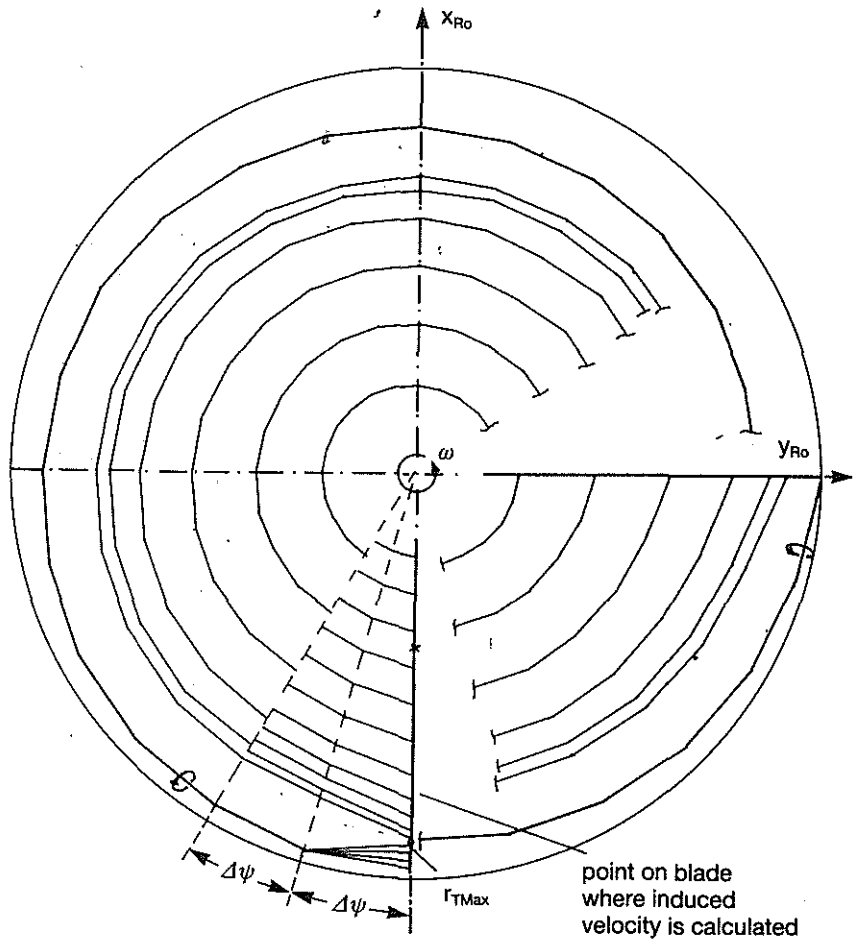

Fig. 16: Vortex Wake Model of 4-bladed Rotor in Hover

The Mach number and the effective angle of attack are determined with the velocity (perpendicular to the blade leading edge) resulting from the components of flight velocity and induced velocity. The lift coefficient and therefore the bound circulation on each radial point can then be found with the help of a 2-D profile polar.

The wake geometry of the vortex model can be divided into three parts.

- The near wake formed by the discrete shed and trailed vortex filaments and extending over an intervall $\Delta\Psi$ (normally 30°). The radial position $r\Gamma_{max}$ where the maximum circulation occurs is of prime importance for the structure of the prescribed wake since all the trailed vortex filaments shed from radial positions greater than $r\Gamma_{max}$ are assumed to roll up into a single concentrated tip vortex filament during the interval $\Delta\Psi$.

- The intermediate wake is formed by the array of trailed vortex filaments shed from all radial positions smaller than $r\Gamma_{max}$ during an interval starting from $\Psi > \Delta\Psi$ and extending over one to two rotor revolutions.

- The far wake consists of the rolled up tip vortices with the circulation strength Γ_{max} (maximum circulation on the blade). It is particularly important for the induced velocity field in Hover and Transition and its influence has to be considered over several rotor revolutions for those flight cases.

For Hover the wake geometry was deduced from detailed parametric measurements on model rotors [8]. The same wake geometry was used for the transition flight calculation by superimposing the component of the flight velocity. For higher advance ratios the position of the shed vortex filaments was determined by superposition of the flight velocity with the induced velocities at the blades while the contraction of the tip vortices was determined by measured vortex traces below the model rotor.

The principle computational arrangement of the vortex model is shown in the flow diagram in Figure 17.

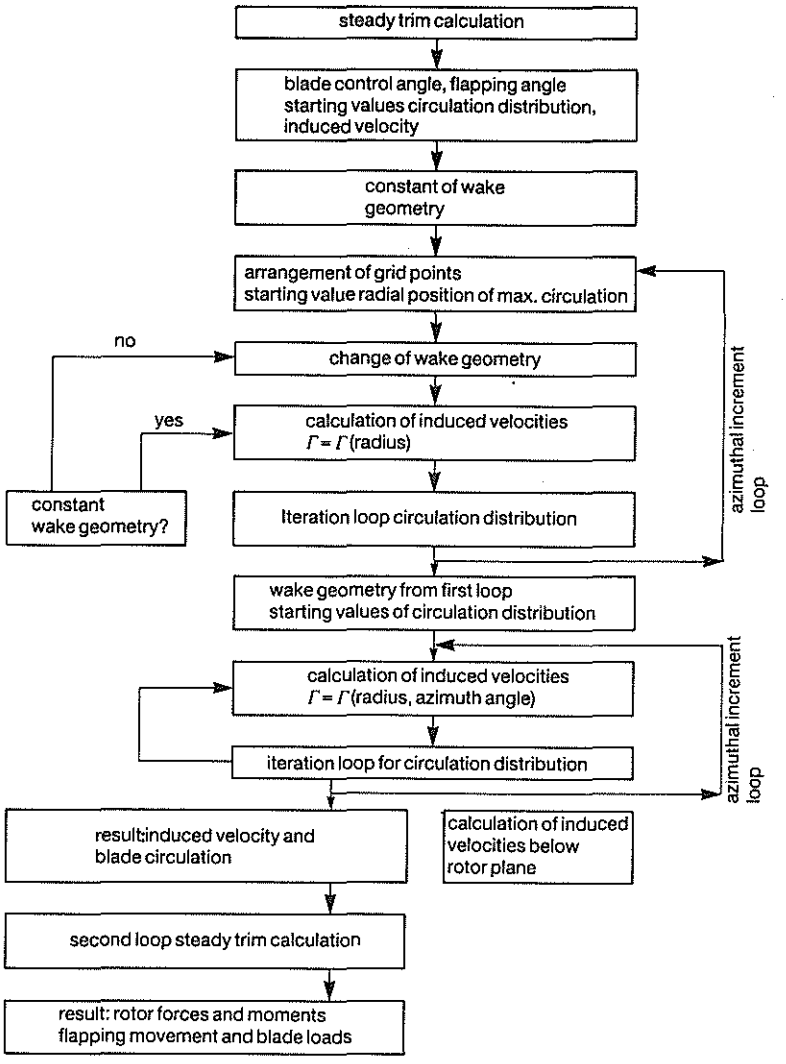

Fig. 17: Flow Chart of Prescribed Wake Model Used for Calculation of Induced Velocities

Before calculating the vortex induced velocities a steady trimmed rotor calculation was done using blade element and local momentum theory. The values thus obtained for bound circulation distribution and induced velocities were used as starting values for the succeeding iteration procedures. As a further input the wake geometry parameters were determined which depend only on rotor geometry and thrust coefficient c_T.

At a fixed azimuth angle an iteration procedure for the radial circulation distribution resulting from the induced velocities at the blade was started which because of its dependence on the point of maximum circulation had to include the wake geometry with the circulation of the trailing vortex filaments being a function of radius only ($\Gamma = \Gamma$ (radius)). In the next program sequence the change of circulation along the shed and trailing vortex filaments was considered ($\Gamma = \Gamma$ (radius, azimuth)) with the assumption that the wake geometry obtained from the first iteration stays constant.
The whole trimmed rotor calculation was finally repeated with the calculated induced velocities at the blade.

In order to compare calculations with the prescribed wake model with direct measurements of induced velocities obtained with hot wires the program had to be modified to calculate the velocities at certain points below the rotor plane which are repeatedly induced in the azimuth interval $2\pi/n$ (n = number of blades). This calculation was done after the determination of the circulation as a function of radial position and azimuth angle was completed.

4. Comparison between measured and calculated downwash distributions

Downwash calculations were done in the rotor disc plane and in a measurement plane 10 cm below the rotor (z/R = 0.05) (Figure 18).

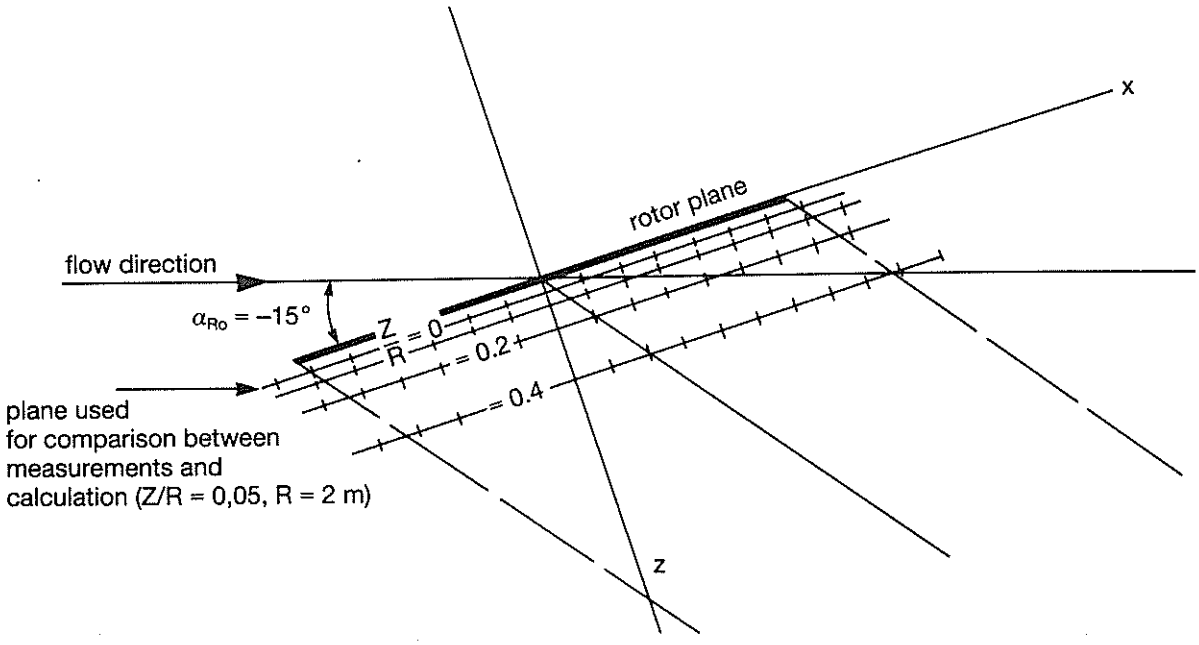

Fig. 18: Arrangement of Measurement Planes below Rotor

Comparison between measurements and calculations in planes further below the rotor plane would have been doubtful because of vortex decay and wake distortion. The comparison was made at fixed radial and azimuthal positions within a circle whose centre coordinates

$$\Delta Z_M = 0.05\ R \quad \text{and} \quad \Delta X_M = - \frac{\Delta Z_M \cdot V_M \cdot \cos \Theta_L}{V_{im} + V_x \cdot \sin \Theta_L}$$

are located on the theoretical wake centre line. In the above equation V_{im} is the z-component of the mean induced velocity and Θ_L is the rotor attitude angle in free flight. The centre coordinates refer to the rotor reference system (x- positive in flight direction, v- positive to the right and z- positive downward). Some uncertainty in the comparison between calculation and measurement was introduced because of a necessary correction for the rotor attitude angle due to wind tunnel wall interference effects.

The basic input parameters for the trimmed rotor calculation necessary for starting the prescribed wake vortex program were obtained from the measured model rotor parameters and quantities listed for all five flight cases below:

	Hover	Transition	Horizontal Flight	Ascending Flight	Descending Flight
μ	0	0.064	0.252	0.146	0.146
θ_0 (°)	14.14	14.0	15.15	14.58	11.67
$\theta_{0.7}$ (°)	7.14	7.04	8.15	7.58	4.67
θ_c (°)	0.23	2.33	1.60	1.96	2.45
θ_s (°)	-0.024	-1.10	-5.02	-2.64	-2.37
α_{Ro} (°)	0.0	-15.0	-10.0	-15.0	-1.9
V_x (m/s)	0	14	55	32	32
v_z (m/s)	0	0	0	-3.5	3.2
RPM (1/min)	1041	1050	1042	1046	1045
ω (1/s)	109.01	110.00	109.12	109.50	109.40
Fx (N)	76	-55	-194	-101	-66
Fy (N)	6	-168	-90	-162	-72
Fz (N)	-3408	-3792	-4038	-3856	-3894
Mx (Nm)	53	36	51	53	36
My (Nm)	19	1	36	13	-7
Mz (Nm)	492.0	478.5	526.0	521.5	261.5
t (°)	16	18	21	20	24
p (bar)	1.010	1.007	1.011	1.005	1.009
N (kW)	53.7	52.6	57.4	57.1	28.6

Table 2:

4.1 Hover

In Figure 19 the comparison between measured and calculated induced velocities beneath the rotor plane shows satisfactory agreement for radial positions less than r/R = 0.7.

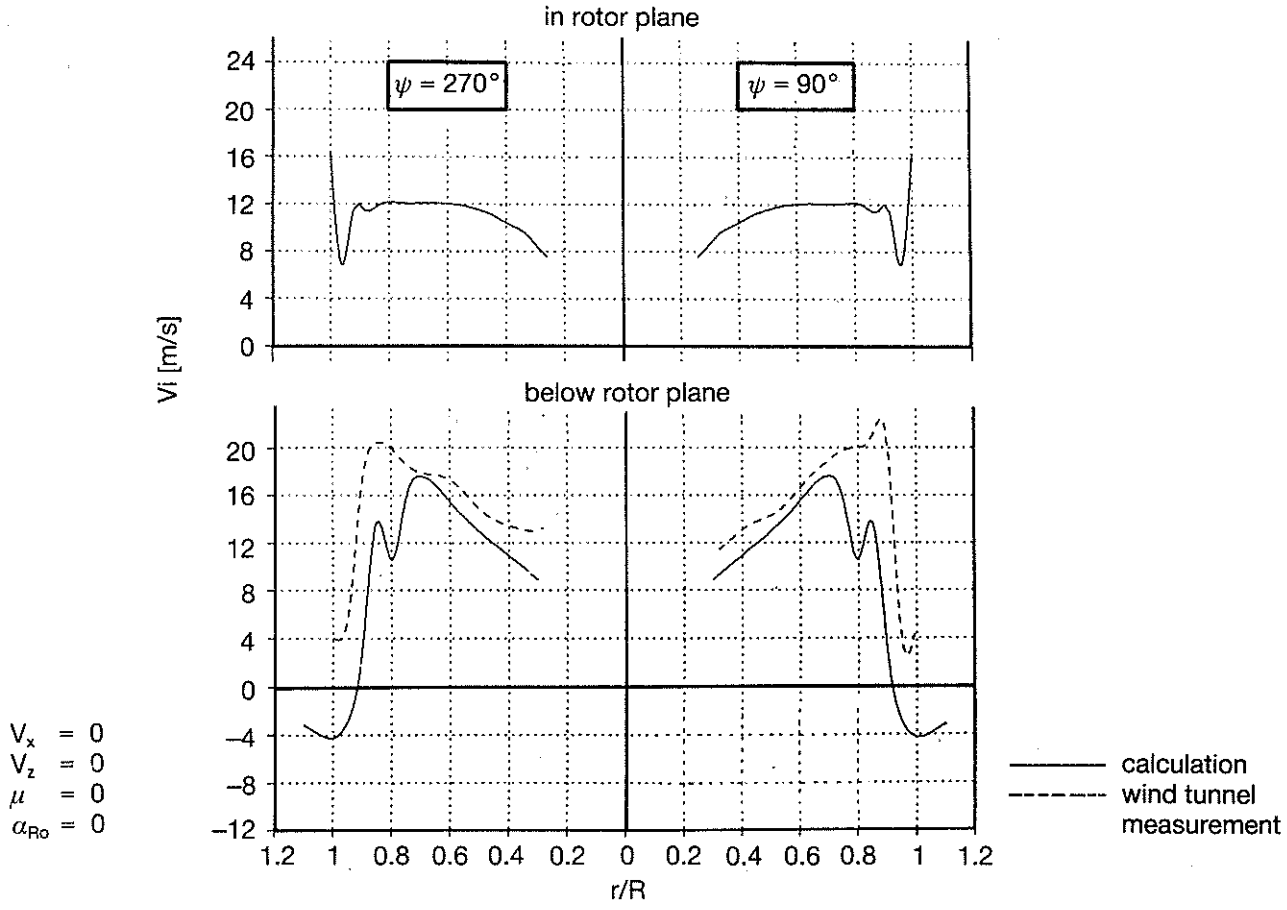

Fig. 19: Induced Velocity Distribution in Hover

The maximum values of the measured induced velocities are however significantly higher and the whole measured velocity distribution profile is displaced radially outward by the amount r/R = 0.05. This last effect is apparently due to the fact that the measured positions of the tip vortices do not coincide with the calculated positions of the tip vortices. Since the semi-empirical wake model is based specifically on well established measured positions of the rolled up tip vortices in Hover the discrepancy is probably caused by different interference effects between rotor and surroundings in the present Hover tests as compared to the Hover measurements that provided the input data for the vortex model.

The calculated induced velocities in the rotor plane show a gradual increase from V_i = 8 m/s near the blade root to a fairly constant value of v_i = 12 m/s between r/R = 0.6 and r/R = 0.9. At r/R > 0.9 there is a sudden drop in the magnitude of the induced velocity caused by tip vortex effects till the downwash values rise again rapidly to values of $v_i \approx$ 16 m/s at the blade tip where the boundary condition of zero lift is applied. This necessary boundary condition was also helpful for eliminating convergence difficulties of the iteration procedures due to

the discretization of the vortex filament array. The considerable difference between the downwash distribution in the rotor plane and underneath the rotor plane (Z/R = 0.05) is mainly caused by the strong vortices shed from the blade tips whose effects are felt much more immediately beneath the rotor than in the rotor plane itself.

4.2 Transition

The agreement between calculation and measurements shown in Figure 20 and 21 is also quite satisfactory.

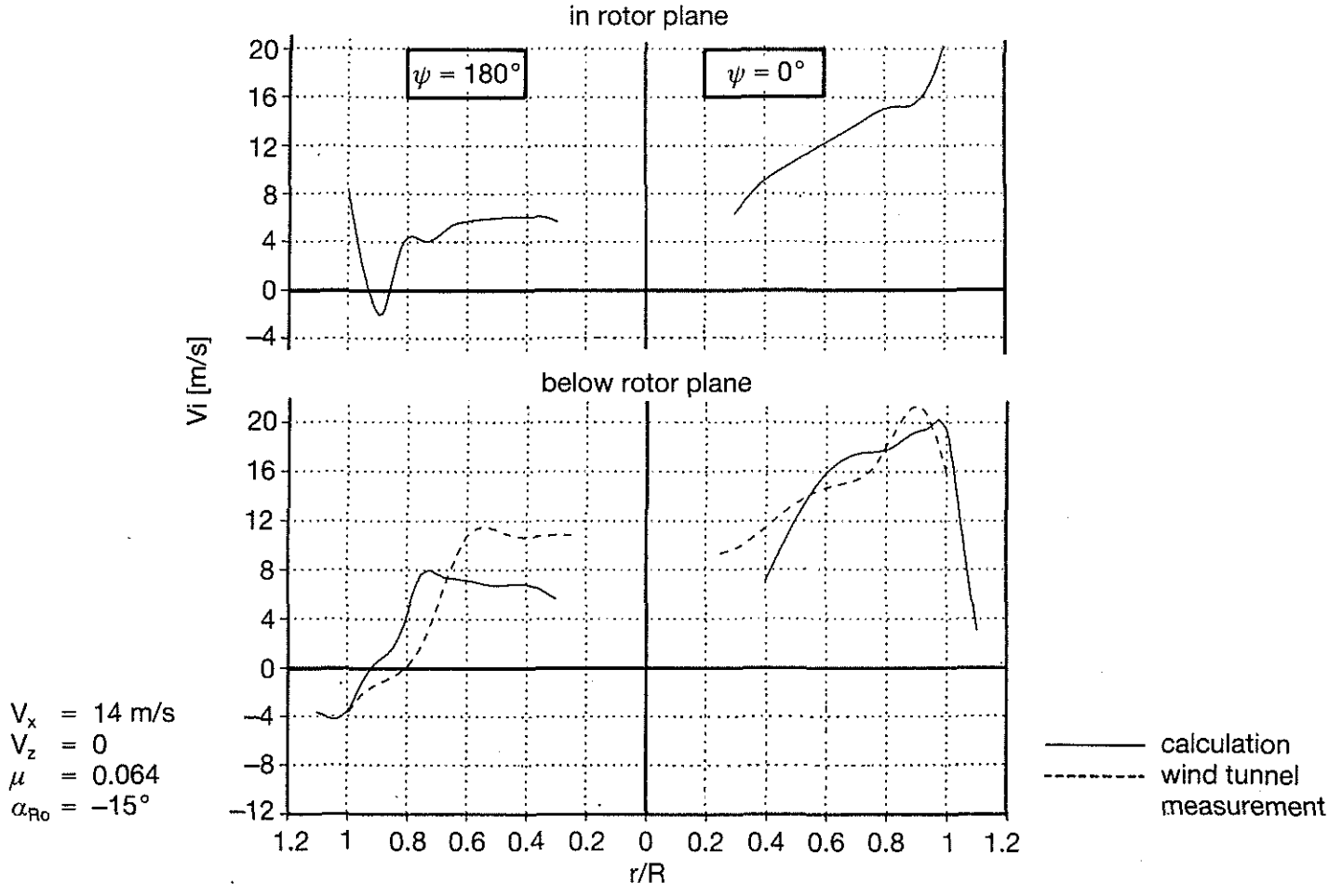

Fig. 20: Induced Velocity Distribution for Transition Flight Simulation Case

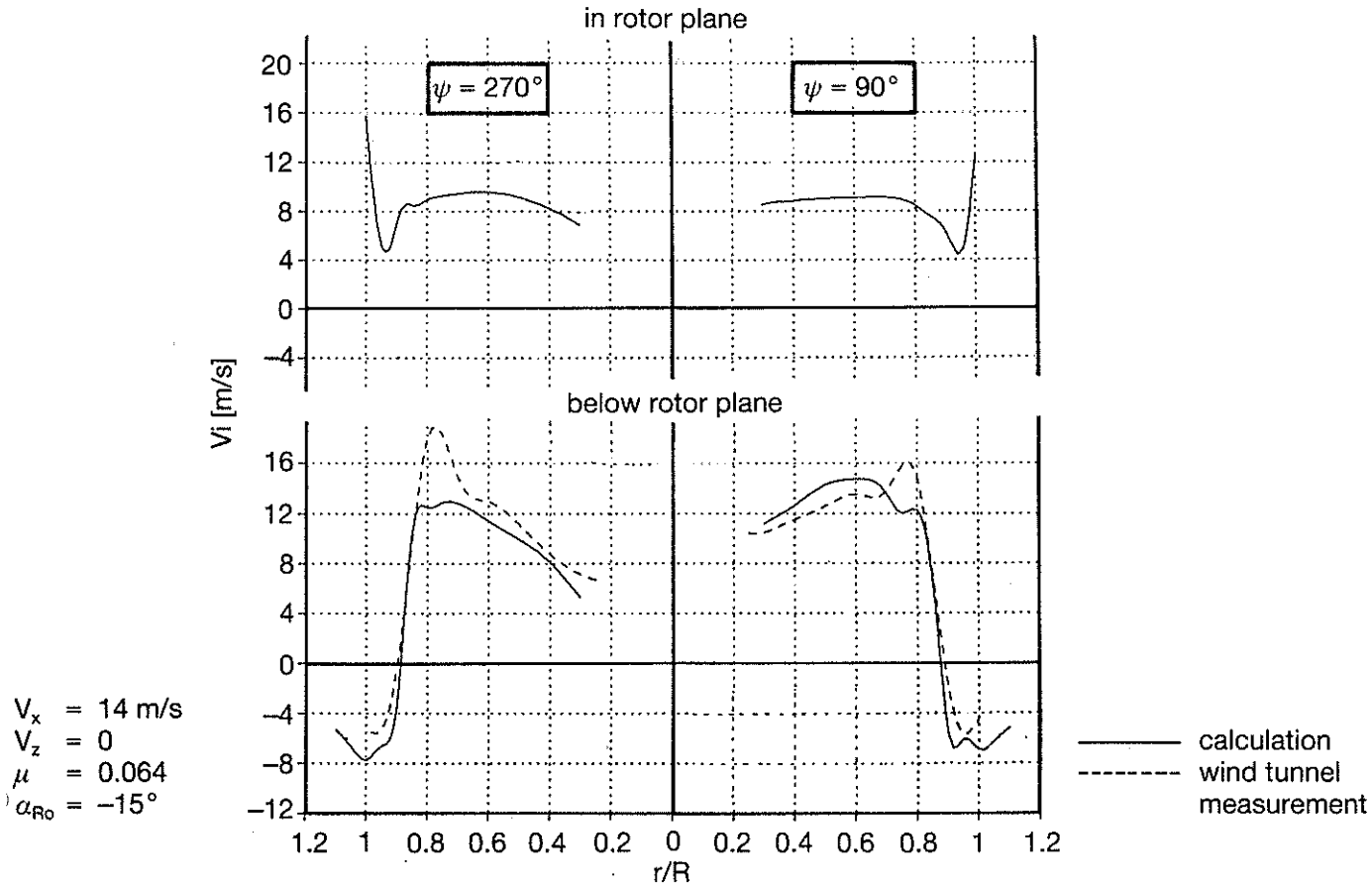

Fig. 21: Induced Velocity Distribution for Transition Flight Simulation Case

The radial section Ψ 90° - 270° (Figure 20) shows that the position and the effect of the vortex next to the measurement plane is well predicted as is also the decrease in magnitude of the induced velocities towards the rotor centre. Only the measured maximum values of the induced velocities are somewhat higher than the calculated ones just as in the hover simulation. The satisfactory agreement between measurement and theory gives some justification to use the empirical wake geometry of the vortex model obtained from Hover tests for the transition flight as well

The difference between the calculated induced velocities at the blade and below the rotor plane are as distinct as in Hover.

Although no direct measurements of induced velocities were possible with hot wires in the rotor plane, the calculated downwash distribution in the rotor plane is considered fairly reliable because of the good agreement between the prescribed vortex model and the measurements beneath the rotor.

4.3 Horizontal Flight

The results for the measured and calculated downwash distributions for the forward flight simulation are shown in Figures 22 and 23.

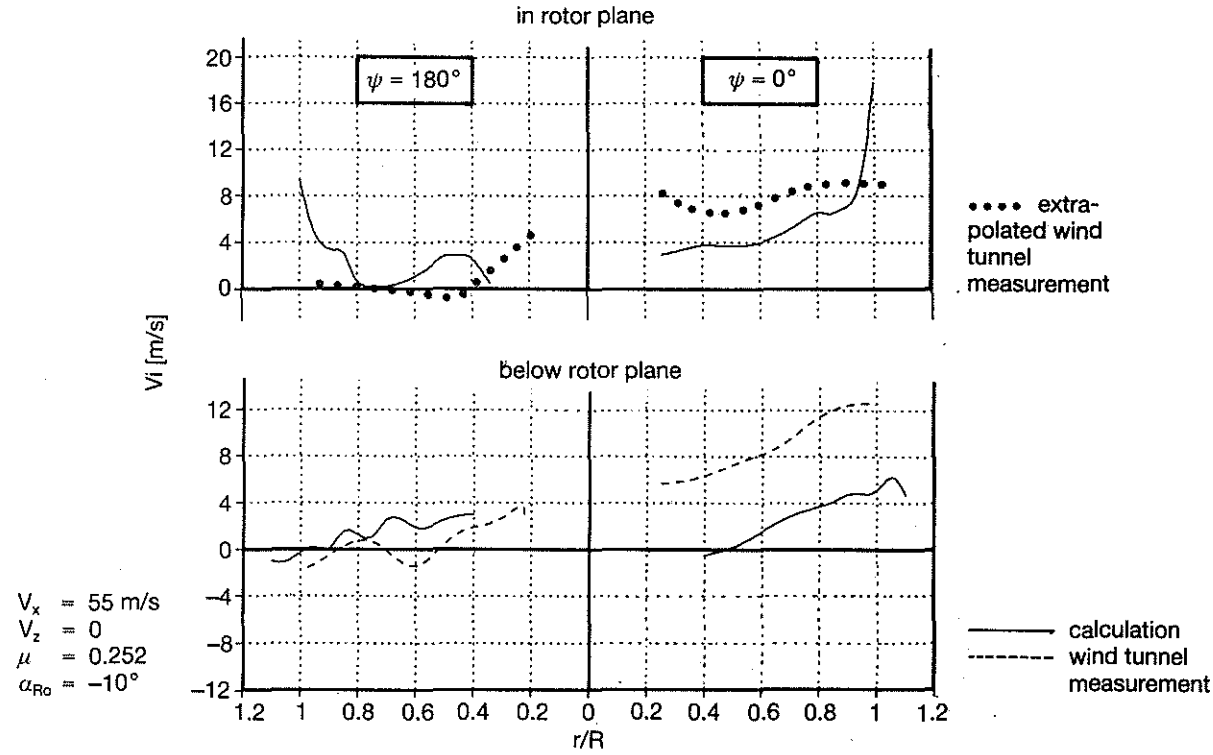

Fig. 22: Induced Velocity Distribution for Horizontal Flight Simulation Case

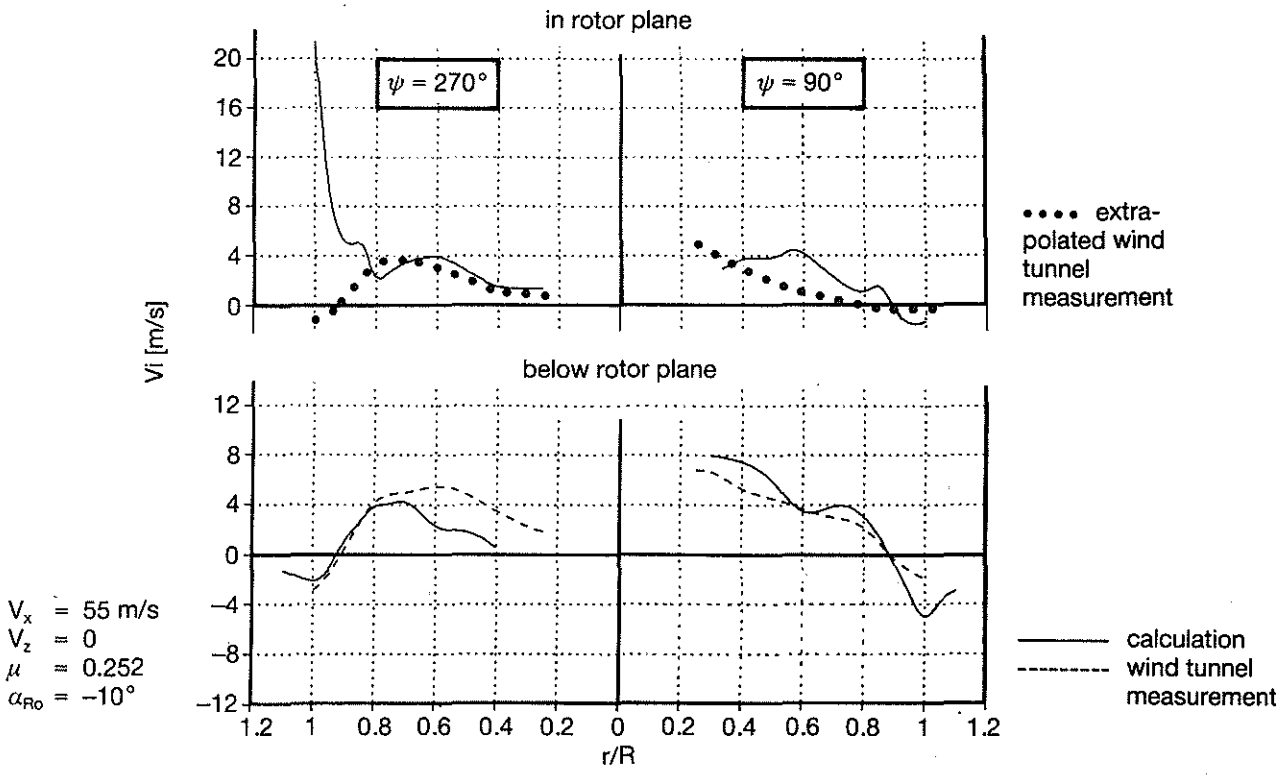

Fig. 23: Induced Velocity Distribution for Horizontal Flight Simulation case

While the calculation of induced velocities below the rotor still contains some tip vortex effects the measurements show a relative smooth radial downwash distribution indicating that the tip vortices in the plane z/R = 0.05 have already been swept downstream by the mean flow through the rotor. An attempt was therefore made to extrapolate the direct downwash measurements in three planes below the rotor (z/R = 0.05/

0.1/ 0.2) into the rotor plane. The extrapolation method was based on a cubic spline interpolation program that made it possible to determine the gradient of the induced velocities perpendicular to the rotor plane for each radial and azimuthal position. The extrapolated measurements are compared in Figures 22 and 23 with the calculated induced velocities. With the exception of the tip region where the boundary condition of zero lift again causes a rapid rise in the predicted downwash the extrapolated measurements confirm the trend of the calculated induced velocities at the blades over most of the radial and azimuthal sections.

4.4 Ascending and Descending Flight

For the ascending flight simulation a comparison between calculation and extrapolated measurements of induced velocities in the rotor plane was made. Figure 24 shows that strong measured tip vortex effects below the rotor are extrapolated into the rotor plane mainly on the advancing and retreating azimuth position and that these vortex effects are not apparent in the calculations.

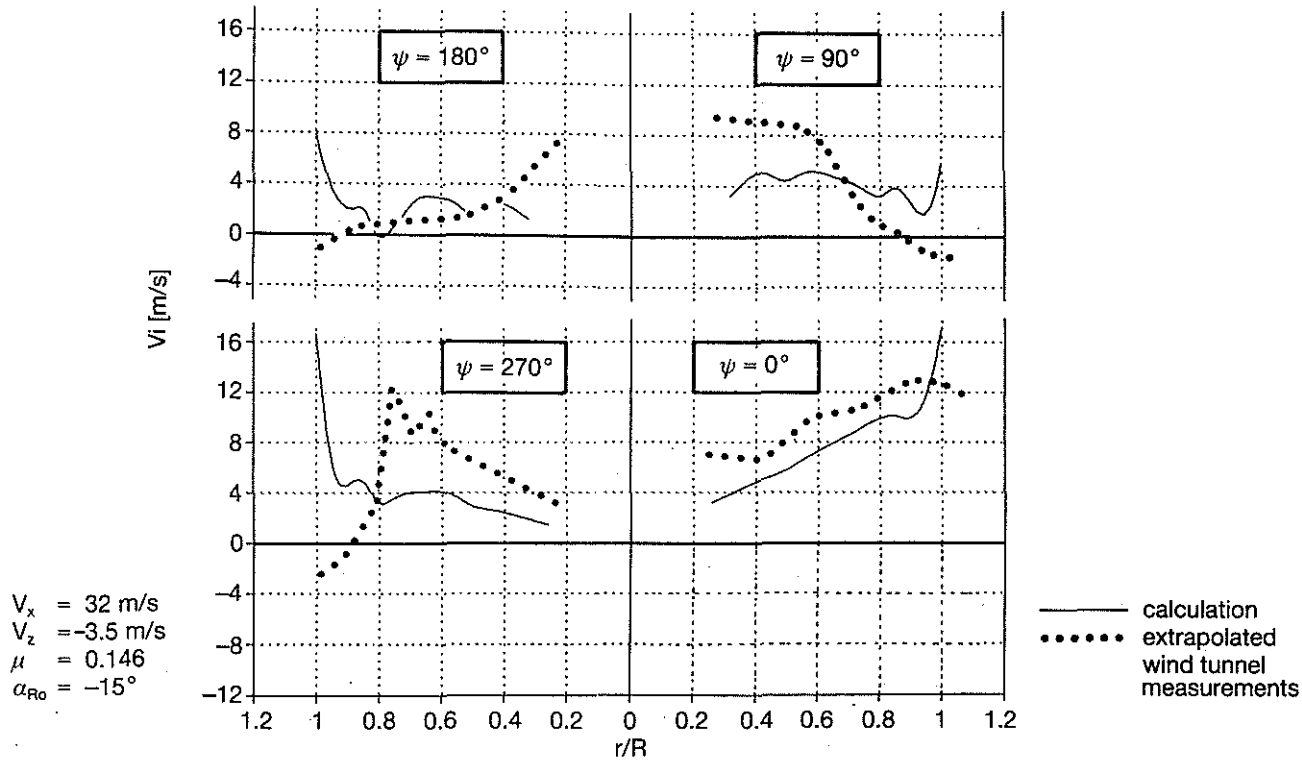

Fig. 24: Induced Velocity Distribution for Ascending Flight Simulation Case

It is concluded that the extrapolation technique of the measurements cannot be applied for the present ascending flight case at a forward velocity of V_x = 32 m/s.

The extrapolation technique gave generally better results for the descending flight case. Although Figure 25 shows that the calculation predicts a somewhat stronger tip vortex effect in the rotor plane for all four azimuth positions shown, the agreement in the order of magnitude and radial trend of the induced velocities between the calculation and the extrapolated measurements is still acceptable.

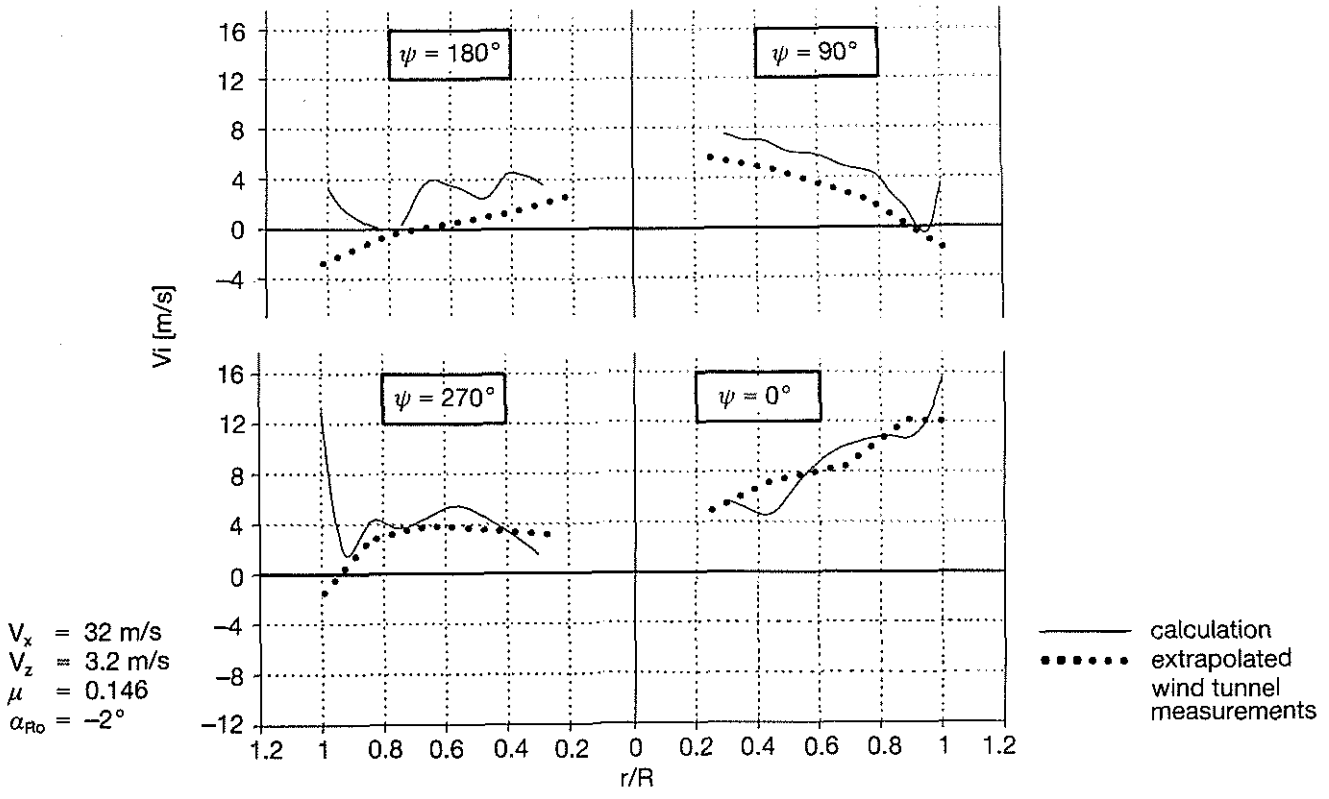

Fig. 25: Induced Velocity Distribution for Descending Flight Simulation Case

For the descending flight it can be expected that the tip vortices stay close to the rotor blades and are therefore not registered by the hot wire sensors in planes below the rotor. This could be an explanation for the fairly smooth downwash distribution of the extrapolated measurements in the rotor plane.

5. Conclusions

- The computer controlled flow alignment technique with triple hot wire probes and the subsequent measurement of the local velocity vector appears to be a powerful and accurate method for rotor downwash determination if the sensors are not directly positioned within vortices that are of the same order of size as the sensor itself.

- To obtain these accurate wind tunnel data in future downwash investigations it is important to keep the interference between the rotor thruflow and the wind tunnel walls to a minimum for example by means of very large test sections or open jet test sections and to use measuring techniques for example laser doppler anemometry or simultaneous hot wire measurements below and above the rotor plane that allow a more precise determination of induced velocities in the rotor plane.

- By keeping model rotor/wind tunnel interference to a minimum and eliminating the need to extrapolate direct measurements, wind tunnel data of induced velocities for a wide range of simulated rotor flight conditions could lead to improved accuray of simple but fast prescribed wake models necessary for routine power calculations and preliminary rotor design work.

References

1. K.H. Horstmann, H. Köster, G. Polz, Improvement of two blade sections for helicopter rotors, Forum Proceedings of the 10th European Rotorcraft and Powered Lift Forum, Paper No. 1, Sept. 1984)

2. B. Junker, Investigations of blade-vortices in the rotor-downstream, Forum Proceedings of the 11th European Rotorcraft and Powered Lift Forum, Paper No. 101, Sept. 1985

3. B. Junker, Investigations of blade vortices in the rotor-downwash, Forum Proceedings of the 12th European Rotorcraft and Powered Lift Forum, Paper No. 101, Sept. 1986

4. R. H. Miller, Rotor Hovering Performance Using the Method of Fast Free Wake Analysis, AIAA-82-0094, Jan. 1982

5. R. H. Miller, Simplified Free Wake Analysis for Rotors, FFA (Sweden), TN 1982-7

6. G. Daske, I.A. Simons, Rotorberechnung mit Berücksichtigung der ungleichförmigen Verteilung der induzierten Geschwindigkeiten, Bölkow GmbH, Bericht DF70, Dez. 1967

7. R. Stricker, W. Gradl, G. Polz, Aerodynamische Arbeitsgrundlagen für zukünftige Hubschrauberentwicklungen (Rotortheorie, Rotorabwind und Interferenz), MBB-Bericht No. UD-159-75 (ZTL 1975, MBB 4.05-7)

8. A. J. Landgrebe, An analytical and experimental investigation of helicopter rotor hover performance and wake geometry characteristics, USAA MRDL TR-71-24, U.S. Army, June 2971